



SPE 75158

An Alternative View of Filter Cake Formation in Fractures

R.S. Seright, SPE, New Mexico Petroleum Recovery Research Center

Copyright 2002, Society of Petroleum Engineers Inc.

This paper was prepared for presentation at the SPE/DOE Thirteenth Symposium on Improved Oil Recovery held in Tulsa, Oklahoma, 13–17 April 2002.

This paper was selected for presentation by an SPE Program Committee following review of information contained in an abstract submitted by the author(s). Contents of the paper, as presented, have not been reviewed by the Society of Petroleum Engineers and are subject to correction by the author(s). The material, as presented, does not necessarily reflect any position of the Society of Petroleum Engineers, its officers, or members. Papers presented at SPE meetings are subject to publication review by Editorial Committees of the Society of Petroleum Engineers. Electronic reproduction, distribution, or storage of any part of this paper for commercial purposes without the written consent of the Society of Petroleum Engineers is prohibited. Permission to reproduce in print is restricted to an abstract of not more than 300 words; illustrations may not be copied. The abstract must contain conspicuous acknowledgment of where and by whom the paper was presented. Write Librarian, SPE, P.O. Box 833836, Richardson, TX 75083-3836, U.S.A., fax 01-972-952-9435.

Abstract

A new model was developed to describe water leakoff from Cr(III)-acetate-HPAM gels during extrusion through fractures. This model is fundamentally different than the conventional filter cake model that was used during hydraulic fracturing. Even so, the model accurately predicted leakoff during extrusion of a guar-borate gel. Thus, the new model may be of interest in hydraulic fracturing.

For a Cr(III)-acetate-HPAM gel, pressure gradients and gel dehydration during extrusion were similar at 20°C, 40°C, 60°C, and 80°C. Similar gel dehydration behavior was observed over a three-fold range of concentration for Cr(III)-acetate-HPAM gels. During extrusion, measurements of pressure gradient versus HPAM concentration paralleled those of elastic modulus versus HPAM concentration.

In 0.04-in.-wide fractures, gel mobilization during brine injection (i.e., gel washout) occurred at pressure gradients similar to those during gel injection. In wider fractures (0.08- and 0.16-in.), Cr(III)-acetate-HPAM gels experienced mobilization at lower than expected pressure gradients. We explored how incorporation of particulate matter into gel affects washout from fractures. Shredded polypropylene and fiberglass insulation dispersed well in Cr(III)-acetate-HPAM gels. In contrast, mica, nut plug, diatomaceous earth, and celloflakes experienced severe gravity segregation. Incorporation of 0.1%-0.2% fiberglass insulation into Cr(III)-acetate-HPAM gels reduced gel washout during subsequent brine injection. However, improved formulations are needed to prevent washout for fractures that are wider than 0.08 in.

Introduction

This work was motivated by an attempt to understand gel propagation through fractures during water shutoff treatments.

Earlier work¹⁻⁵ revealed that gels lost water during extrusion through fractures and that water leakoff from the gel controlled the rate of gel propagation. Leakoff was also known to control the rate of fracture growth during hydraulic fracturing⁶⁻¹⁰ and during produced water re-injection.¹¹⁻¹³

In the conventional view of hydraulic fracturing, the rate of leakoff was determined by one (or a combination) of three mechanisms^{6,8,9}: (1) propagation of the fracturing fluid front into the rock matrix (i.e., away from the fracture face), (2) reservoir fluid viscosity/compressibility effects, and (3) the formation of a filter cake associated with particulate matter that was suspended in the fracturing fluid. The latter mechanism may involve formation of a filter cake on the fracture surface (i.e., an external filter cake) and/or penetration of the particulates some distance into the porous rock (i.e., an internal filter cake). This paper focuses on leakoff that is dominated by the formation of an external filter cake in a fracture. We will first review the conventional filter cake model. Second, experimental evidence will be presented that questions a key assumption of the conventional model. Next, an alternative model will be presented. Then, important differences in predictions from the models will be discussed, especially with respect to shear rates and stress levels in the fracture during fluid flow. This paper also examines gel behavior in fractures as a function of temperature, gel composition, and brine injection after gel placement.

Conventional Filter Cake Model

The widely accepted model of filter cake formation was introduced by Carter.^{6,7,9} Assume that a particulate-laden fluid contacts a rock interface (i.e., a fracture face) and a pressure difference, Δp , exists between the fracture and the porous rock. As solvent (with viscosity, μ) flows into the rock at a velocity, u_f , the particulates form a filter cake of permeability, k , and thickness, L . At any given time, the filtrate velocity (i.e., the leakoff rate) is given by the Darcy equation.

$$u_f = k \Delta p / (\mu L) \dots\dots\dots (1)$$

The thickness of an incompressible filter cake grows at a rate that is proportional to the throughput of filtrate:

$$L = \int u_f dt / \alpha, \dots\dots\dots (2)$$

where α indicates the factor by which the particulates are concentrated during the transition from the suspension to the filter cake. Combining Eqs. 1 and 2 yields Eq. 3.

$$u_i = \alpha k \Delta p / (\mu \int u_i dt) \dots\dots\dots (3)$$

Eq. 4 presents a solution to Eq. 3.

$$u_i = [\alpha k \Delta p / (2 \mu)]^{0.5} (t - t_{exp})^{-0.5} \dots\dots\dots (4)$$

where t_{exp} is the time of first exposure to filter cake for the element of fracture face of interest. The key result in Eq. 4 is that the leakoff rate is proportional to $t^{-0.5}$. This proportionality was often verified experimentally—especially during static filtration experiments.^{6,8,9} An important assumption in the development of Eq. 4 was that the thickness of the filter cake was uniform at any given time. The next two sections will present evidence that questions this assumption.

Gel Behavior in Fractures

Before gelation, fluid gelant solutions can readily leakoff from fractures into porous rock.¹⁴ However, after gelation, the crosslinked materials will not penetrate significantly into the porous rock.¹⁻⁵ Thus, formed gels must extrude through fractures during the placement process. Cr(III)-acetate-HPAM gels (as well as other gels) concentrate or lose water during extrusion through fractures, reducing the rate of gel propagation.¹⁻⁵ When large volumes of gel were extruded through a fracture, the effluent had the same appearance and a similar composition as those for the injected gel, even though a concentrated, immobile gel formed in the fracture. During gel extrusion, water leaked off from the gel, and the gel concentrated to become immobile in the vicinity where dehydration occurred. Crosslinked polymer did not penetrate significantly into the porous rock. The driving force for gel dehydration (and water leakoff) was the pressure difference between the fracture and the adjacent porous rock. Fresh gel (i.e., mobile gel, with the original composition) wormholed through the concentrated gel in order to advance the gel front. With time at a given position along the fracture, the average gel concentration increased and the fracture area contacted by wormholes (i.e., mobile gel) decreased. Even so, water leakoff from the concentrated, immobile gel was generally small compared with leakoff from the mobile gel. During gel extrusion through a fracture of a given width, the pressure gradients along the fracture and the dehydration factors were the same for fractures in 650-mD sandstone as in 50-mD sandstone and 1.5-mD limestone.¹⁻⁵

For a Cr(III)-acetate-HPAM gel, dehydration was quantified for a significant range of conditions.¹⁻⁵ For fracture widths from 0.02 to 0.16 in., fracture lengths from 0.5 to 32 ft, fracture heights from 1.5 to 12 in., and injection fluxes from 129 to 66,200 ft/d, the average rate of gel dehydration and leakoff (u_i , in ft/d or ft³/ft²/d) was described reasonably well using Eq. 5.

$$u_i = 0.05 t^{-0.55} \dots\dots\dots (5)$$

where t is time in days. Fig. 1 summarizes the results.⁵

On first consideration, Eq. 5 and the dashed line in Fig. 1 appeared to support the conventional view of filter cake formation in hydraulic fractures (i.e., because leakoff varied with $t^{-0.5}$ as suggested by Eq. 4). However, the conventional model assumed that a uniform filter cake formed. In contrast, our experiments revealed that fresh gel wormholed through concentrated gel—resulting in a distinctly non-uniform distribution of the filter cake on the fracture faces. Fig. 2 shows the wormhole pattern that developed during one experiment.⁴ Early in the process of gel injection, the wormhole pattern was very branched, with a significant fraction of the fracture area contacted by the wormholes (as in Fig. 2).⁴ As additional gel volumes were injected, the wormholes became less branched, and a diminished fraction of the fracture area was contacted by the wormholes.⁴ This behavior was not surprising since the dehydrated gel became increasingly concentrated and less mobile and the mobility ratio (mobility of fresh gel divided by mobility of concentrated gel) increased with gel throughput.

New Mechanistic Model for Leakoff

The above observations inspired a new mechanistic model of gel propagation and dehydration in fractures. Consistent with our experimental results, this model assumed the following:

1. Water can leave the gel and leakoff through the fracture faces, but crosslinked polymer cannot.
2. The mobile gel has the same composition as the injected gel.
3. When an element of mobile gel dehydrates, that gel becomes immobile. For a given vicinity and time, t , in a fracture of width, w_f , the average gel concentration (C/C_o , which gives the gel concentration, C , relative to the concentration for the injected gel, C_o) is

$$C/C_o = 1 + \int u_i dt / w_f \dots\dots\dots (6)$$

where u_i is the average leakoff rate for that vicinity.

4. At a given point along the fracture, the fracture surface is covered by either mobile gel (with fractional area, A_m) or immobile gel (with fractional area, A_c) so that

$$A_m + A_c = 1 \dots\dots\dots (7)$$

The fraction of surface that contacts mobile gel decreases with time as more immobile gel forms. Based on area and mass balances, the fractional area covered by concentrated gel at a given time and vicinity is approximated by

$$A_c = [C/C_o - 1] / [C/C_o] \dots\dots\dots (8)$$

Presumably, as mobile gel in a wormhole dehydrates, a thin layer of concentrated gel forms at the fracture surface. However, this thin layer is continually pushed aside by the

leakoff water or mobile gel, and the concentrated gel is added to the accumulation of immobile gel at the sides of the wormhole.

- Water leakoff from immobile (dehydrated) gel (u_c) is negligible compared to that from the mobile gel (u_m). (The immobile gel continues to concentrate and lose water with time. However, this leakoff rate is small compared to that from the much more permeable mobile gel. The validity of this assumption was demonstrated in Ref. 4.)

$$u_m \gg u_c \dots\dots\dots (9)$$

- The mobile gel has a finite permeability to water (k_{gel}) that provides a fixed local leakoff flux (u_m) for the fracture surface that is in direct contact with mobile gel (i.e., the wormhole area that is in contact with the fracture faces).

$$u_l \approx A_m u_m \dots\dots\dots (10)$$

Combining Eqs. 6 to 10 yields Eq. 11, which is the basis of the new model. The model predicts the leakoff rate (i.e., the rate of gel dehydration) at a given time and distance along the gel-contacted portion of a fracture.

$$u_l = u_m / [1 + \int u_l dt / w_f] \dots\dots\dots (11)$$

The denominator of Eq. 11 reflects the rate of loss of fracture surface that is contacted by mobile gel (i.e., the wormhole-contact area). For our 24-hr-old Cr(III)-acetate-HPAM gel, u_m has a value around 4 ft/d, which translates to a k_{gel} value around 1 mD. The latter value was confirmed from independent experiments.¹⁵ The fraction of the fracture area that was contacted by concentrated gel versus time is plotted in Fig. 3. This plot indicates that after 0.0007 days (1 minute) of gel contact, at least 50% of the fracture face is covered by concentrated gel rather than fresh gel. Within 0.02 days (30 minutes) of gel contact, more than 90% of the fracture face is covered by concentrated gel.

Leakoff predictions from Eq. 11 are plotted in Fig. 1 (solid line), and these predictions match the experimental data quite well. In view of the similarity of Eqs. 3 and 11, the similarity of leakoff predictions is not surprising. However, the two models predict significantly different flow and leakoff patterns and shear rates and stress levels within a fracture. These differences have important consequences for erosion of the filter cake, propagation of gels and particulates along fractures, transmission of pressures along fractures, fracture extension, and gel washout after placement.

Model Differences

In the conventional model, the thickness of the filter cake is areally uniform (at least locally); the entire fracture area continually experiences leakoff; and the leakoff rate decreases because of a steady growth in thickness of the filter cake. In the new model, the filter cake is areally heterogeneous; leakoff is significant only on the fracture area that is contacted by

wormholes; and the global leakoff rate decreases because of a continual loss of fracture area that is contacted by wormholes.

In the conventional model, a single opening to flow exists that has a width (w_c) that is equal to the fracture width minus twice the thickness of the filter cake at that point. The height of this opening is basically as high as the fracture. Thus, the flow opening is extremely high and narrow. In contrast, in the new model, for a given distance along the fracture, multiple flow channels exist (corresponding to the wormholes), the width of each channel (w_w) could be only slightly less than the original fracture width, and the “height” of each channel is small compared to the total fracture height (but generally large compared to the fracture width).

Using the methods described in Ref. 16, one can readily show that for a Newtonian fluid, the shear rate at the wall, γ_w , in a slit of width, w , is given by Eq. 12

$$\gamma_w = (w dp/dl) / (2 \mu_o) , \dots\dots\dots (12)$$

and the average fluid velocity, u_{ave} , is given by Eq. 13

$$u_{ave} = (w^2 dp/dl) / (12 \mu_o) , \dots\dots\dots (13)$$

where dp/dl is pressure gradient along the fracture and μ_o is fluid viscosity.

For power-law fluids, shear stress, τ_{xz} , is given by Eq. 14,

$$\tau_{xz} = K (\gamma)^{n+1} , \dots\dots\dots (14)$$

the shear rate at the wall is given by Eq. 15

$$\gamma_w = [(w dp/dl) / (2 K)]^{1/(n+1)} , \dots\dots\dots (15)$$

and the average fluid velocity is given by Eq. 16

$$u_{ave} = [dp/dl / K]^{1/(n+1)} (w/2)^{(n+2)/(n+1)} (n+1)/(2n+3) \dots\dots\dots (16)$$

K is the consistency index, and n is the power-law exponent.

For both the Newtonian and power-law fluids, the shear stress at the wall, τ_w , is

$$\tau_w = w dp/dl / 2 \dots\dots\dots (17)$$

Eqs. 12-17 can be used to compare predictions from the conventional model and the new model.

To make this comparison, consider the case where the two models are given the same total leakoff volume, and consequently, the same total volume of filter cake. Because the total fracture height is fixed, the total cross-section that remains open to flow must be the same for the two models. Based on Eqs. 14-17, Table 1 compares predictions (for a power-law fluid) for shear rate at the wall, average fluid velocity, shear stress at the wall, and pressure gradient from the two models. The listings compare predictions from the new model relative to those from the conventional model. Remember that w_w/w_c will always be greater than one—and

usually much greater than one. Also, n is zero for a Newtonian fluid and could be -0.9 for a strongly shear-thinning fluid.

For a fixed pressure gradient, the new model predicts higher shear rates and shear stresses at the wall and much higher average fluid velocities than the conventional model. Therefore, greater erosion of the filter cake is predicted in the new model than in the conventional model.

In contrast, if the injection rate is held constant, the new model predicts much lower pressure gradients along the fracture than that predicted by the conventional model. Of course, the pressure gradient along the fracture impacts gel propagation and gel washout in water-shutoff treatments and fracture extension in hydraulic fracturing and produced water re-injection (i.e., by affecting the pressure at the fracture tip).

Pressure Gradients During Gel Propagation

For Cr(III)-acetate-HPAM gels, a minimum pressure gradient was required to extrude the gel through a fracture with a given width.¹ Once this minimum pressure gradient was exceeded, the pressure gradient during gel extrusion was insensitive to the flow rate. For example, in a 0.04-in.-wide fracture, a 1-day-old gel with 0.5% HPAM and 0.0417% Cr(III)-acetate exhibited a pressure gradient that averaged 28 psi/ft for injection fluxes between 413 ft/d and 33,100 ft/d.³ Mechanical degradation of the gel was fairly small. For gel produced from the fracture at the highest rate, the elastic modulus was about 20% less than that for the original gel. In all cases, the physical appearance of the gel remained unchanged by passage through the fracture.

For fractures with widths between 0.006 and 0.4 in., the pressure gradient required for gel extrusion varied roughly inversely with the square of fracture width (see Fig. 4).^{1,2} This behavior was directly tied to the insensitivity of pressure gradient to changes in flow rate. Ref. 4 demonstrated mathematically that if pressure gradient is independent of flow rate (for a fracture with a given width), the pressure gradient should vary inversely with the square of fracture width.

Effect of Temperature

Most of our experiments to date were performed at 41°C. Of course, many reservoirs and field applications exist at other (mostly higher) temperatures. Therefore, a need exists to determine gel extrusion and dehydration properties at other temperatures. Using temperatures ranging from 20°C to 80°C, extrusion experiments were performed using 650-mD Berea sandstone cores that had lengths of either 6 or 48 in. In each case, the fracture width was 0.04 in. and the fracture height was 1.5 in. Pressure taps along each four-ft-long fracture divided the core into five sections of equal length. A single set of pressure taps were used for the 6-in.-long fractures. Effluent from the fracture and matrix were collected separately. We used our standard Cr(III)-acetate-HPAM gel (0.5% Alcoflood 935 HPAM, 0.0417% Cr(III) acetate) that was aged for 24 hours at 40°C before injection. The fractured core was equilibrated at the test temperature well before gel injection started. During injection of 226 in.³ (3.7 liters) of gel, the rate was fixed at 122 in.³/hr (2,000 cm³/hr)—translating to a flux

in the fracture of 4,130 ft/d. Leakoff results from six sets of experiments are shown in Fig. 5. This figure shows that the leakoff behavior was not sensitive to temperature between 20°C and 80°C. The pressure gradients during gel extrusion were insensitive to temperature for these experiments.⁵ The elastic modulus (G') of this gel was also independent of temperature.¹⁷ In contrast, the viscosity of water decreased by a factor of ~ 3 as temperature increased from 20°C to 80°C.

For times shorter than 0.01 days (15 minutes), the leakoff data were very consistent with the predictions from our new leakoff model (solid curve in Fig. 5). For times longer than 0.01 days, the leakoff results exceeded the predictions associated with the new model, especially for the shorter cores. We suspect that this deviation was an artifact associated with the use of short fractures. In particular, some of the concentrated gel may be dislodged and produced from short fractures—thus, permitting greater wormhole-fracture surface areas and higher leakoff rates for longer time periods. In longer fractures, the effect was less noticeable, although some deviation was noted at 40°C and 60°C (see Fig. 5).

Effect of Gel Composition

Experiments were performed to investigate how gel extrusion and dehydration vary with gel composition. Most of our previous work used our “1X” gel that contained 0.5% HPAM, 0.0417% Cr(III) acetate, 1% NaCl, and 0.1% CaCl₂. Recently, we tested a series of five compositions, including 1X, 1.5X, 2X, 2.5X, and 3X Cr(III)-acetate-HPAM gels. The multiplier refers to the HPAM and chromium concentrations relative to those in our standard 1X gel. In all cases, the HPAM/Cr(III)-acetate ratio was fixed at 12/1, and the gels were aged for one day at 40°C before injection at 4,130 ft/d (2,000 cm³/hr) into 6-in.-long, 1.5-in.-diameter Berea sandstone cores that each contained a 0.04-in.-wide fracture. Because high-pressure gradients were anticipated during extrusion of the concentrated gels, we used 6-in.-long cores that were cast in a metal alloy. Our 48-in.-long cores (that were cast in epoxy) would not withstand the required pressures.

Leakoff results from these five experiments are plotted in Fig. 6. Interestingly, the gels showed similar leakoff behavior. Predictions from the new model matched the leakoff results quite well for times less than 0.01 days. However, for longer times, the leakoff results exceeded the predictions. As mentioned earlier, this deviation may be an artifact associated with the use of short fractures.

Pressure gradients during gel extrusion for the five experiments are plotted using solid circles in Fig. 7. This figure also plots the quantity, $2G'/w_f$, using open circles. The elastic modulus, G' , was measured over a range of gel compositions using a Paar-Physica Model UDS 200 Dynamic Spectrometer.¹⁷ Based on a force balance, the quantity, $2G'/w_f$, should predict the pressure gradient required to extrude a gel through a fracture of a given width.¹⁷ Fig. 7 reveals that this force-balance approach typically under-predicts the pressure gradient by a factor of 87. Thus, more work is needed to relate rheological measurements to our extrusion results. However,

the G' measurements paralleled the extrusion pressure gradients when plotted versus gel composition. In Fig. 7, $2G'/w_f$ increased with $e^{2.27\%HPAM}$ (where %HPAM indicates the HPAM concentration in the gel). Also, for the lower four gel compositions (1X to 2.5X), the pressure gradient for gel extrusion also varied with $e^{2.27\%HPAM}$.

We examined whether the new leakoff model would work as well for a guar-borate gel that was commonly used during hydraulic fracturing. The gel contained 0.36% guar, 0.018% NaBO₂, 0.24% tallow soap, and 0.1% surfactant. This gel was aged for 1 day at 40°C and injected at 4,130 ft/d through a 6-in.-long, 0.04-in.-wide fracture. The experimental leakoff rates (Fig. 8) were matched very well using our new model, even though the new model was developed to match the behavior of Cr(III)-acetate-HPAM gels. As with the Cr(III)-acetate-HPAM gel, the pressure gradient during extrusion of the guar-borate gel (through a second 6x1.5x0.04-in. fracture) was insensitive to rate (i.e., pressure gradient rose by a factor of 2.3 as injection flux increased from 206 and 33,000 ft/d). Another similarity was noted when the experiment illustrated in Fig. 2 was repeated using the guar-borate gel. As with the Cr(III)-acetate-HPAM gel, a wormhole pattern was observed.

Bingham Model of Pressure Behavior

The model presented earlier was quite successful in explaining the leakoff behavior during gel extrusion through fractures. However, this model did not address the pressure behavior during extrusion. We considered whether a Bingham model might be appropriate when describing the pressure gradients. In the Bingham rheological model,¹⁶ the fluid does not move until a minimum shear stress or “yield” stress is exceeded. Above this minimum shear stress, the model assumes that flow is basically Newtonian. In the Bingham model, the fluid velocity profile is flat (the velocity gradient is zero) between the center of the fracture and some distance, x_o , from the fracture center. In other words, the gel flows like a solid plug in this region. Between x_o and the fracture wall, the Bingham model assumes Newtonian flow. In effect, the Bingham model assumes that a Newtonian fluid flowing near the fracture wall lubricates the flow of the plug through the fracture. In our experiments, since the gel dehydrates as it extrudes through fractures, the water leaving the gel during the dehydration process could be the key component of the lubricating layer.

Since the Bingham model assumed Newtonian flow in the lubricating layer, the pressure gradient (above the yield point) should have increased in direct proportion to flow rate if the lubricating layer had a fixed thickness. However, since the pressure gradient was insensitive to flow rate, the lubricating layer apparently increased with increased flow rate. Based on the observed pressure-gradient/flow-rate behavior and the Bingham model, an analysis was performed to estimate the thickness of the lubricating layer relative to the fracture width.¹⁸ The analysis suggested, first, that the thickness of the lubricating layer was very small (relative to the fracture width) for most practical conditions. Second, the thickness of the

lubricating layer increased (almost linearly) with increased superficial velocity.¹⁸

Why should the lubricating layer increase in thickness with increasing velocity? One could argue that the lubrication layer resulted from destruction of the crosslinked-polymer matrix that held water in the gel. Movement of the gel mass in the fracture may require rupture of the outer-most layer of the mobile gel mass. This rupture released the water that served to lubricate movement of the gel mass. The amount of gel disrupted and the volume of water released from the gel may be directly proportional to the distance of gel movement. As velocity of the central gel mass increased, a greater volume of water was released (for a given time period), thereby creating a thicker lubricating layer.

Two flaws exist with the above mechanism. First, the pressure gradients predicted by this model should depend on the viscosity of the “lubricating” fluid (i.e., water in this case). Since the viscosity of water decreased by a factor of about three as temperature rose from 20°C to 80°C and since the elastic modulus of the gel was insensitive to temperature¹⁷, the proposed mechanism predicts that the pressure gradient for gel extrusion should have decreased by roughly a factor of three between 20°C and 80°C. In reality, the pressure gradient was insensitive to temperature over this range.⁵

The second flaw concerns the leakoff behavior. The above mechanism predicts that the lubrication layer should have increased with increased flow rate. With a thicker lubrication layer (i.e., more water), the leakoff rate should have increased with increased extrusion rate. Instead, we observed that the leakoff rate was basically independent of flow rate—it primarily depended on time (see Fig. 1). In view of these deficiencies, we seek an alternative to the Bingham model.

Gel-Slipping-Within-Gel Model

As mentioned in the “Effect of Gel Composition” section, a simple force balance predicted that the pressure gradient for gel extrusion should be given by Eq. 18.

$$dp/dl = 2G'/w_f \dots\dots\dots (18)$$

Two observations appear inconsistent with this equation. First, the pressure gradient for gel extrusion varied inversely with the square of fracture width (see Fig. 4) rather than inversely with fracture width. Second, Eq. 18 under-predicted the pressure gradient by a factor of 87 (see Fig. 7).

To resolve these discrepancies, a second model was considered, which we call the “Gel-Slipping-Within-Gel” model. In this model, Eq. 18 was assumed correct if the fracture width is replaced with an effective channel width that was open to gel flow (or extrusion), w_w . Consequently, this width was determined using Eq. 19 and the experimentally measured pressure gradient, dp/dl .

$$w_w = 2G'/(dp/dl) \dots\dots\dots (19)$$

The data from Fig. 4 were used as input for Eq. 19 to generate Fig. 9. The solid circles and line in this figure indicate that the effective width of the gel flow channel increased with the 1.6 power of fracture width. The open triangles show $(w_f - w_w)/w_f$, the fraction of the fracture width that was occupied by non-flowing gel. This data set indicates that in fractures with widths less than 0.2 in., the flow channels (i.e., the wormholes for the flowing gel) were narrow relative to the total width. In other words, most of the fracture width was occupied by non-flowing gel. On first consideration, this prediction appears in contradiction to physical observations of the wormholes—i.e., the wormholes had about the same widths as the fractures. However, it is possible that much of a given wormhole was occupied by non-flowing gel that had the same composition as the flowing gel. This gel, along with the flowing gel, was still much more permeable than the concentrated gel, and acted as the dominate source of water for leakoff. Of course, more work is needed to understand the pressure behavior during gel extrusion through fractures.

Gel Washout During Brine Injection

Cr(III)-Acetate-HPAM Gel. In many field applications, gel treatments were less effective than expected in reducing water production from fractured wells. Concern exists about the ability of gels to resist washout after placement. During brine flow after gel placement in a fracture, what pressure gradient is needed to re-mobilize the gel? To address this question, several experiments were performed where brine was injected at various rates after gel placement. In all cases, the core material was 650-mD Berea sandstone, with a fracture placed lengthwise down the middle of each core. In each fractured core, 226 in.³ (3.7 liters) of one-day-old Cr(III)-acetate-HPAM gel were injected using a rate of 122 in.³/hr (2,000 cm³/hr). After gel placement, the core was shut in for one day. (These experiments were performed at 41°C.) Next, brine was injected at a low rate (e.g., 6.1 in.³/hr or 100 cm³/hr). A steady state was quickly established, and the pressure gradient was recorded. Then the brine injection rate was doubled, and the measurements were repeated. This process was repeated in stages up to a final brine injection rate of 976 in.³/hr (16,000 cm³/hr). Then the brine injection rate was decreased in stages.

Representative results were obtained using our standard 1X gel in a fracture with a width of 0.04 in. To a first approximation, the pressure gradient for gel failure was the pressure gradient for gel extrusion through the fracture. The solid circles in Fig. 10 show that during gel injection (at 4,130 ft/d effective velocity in the fracture or 2,000 cm³/hr), the pressure gradient rapidly rose to 17 psi/ft during the first 0.7 fracture volumes of gel injected. Thereafter, the pressure gradient was fairly stable during the course of injecting another 80 fracture volumes of gel. When brine was subsequently injected (at 206 ft/d or 100 cm³/hr), the pressure gradient rapidly increased to 16 psi/ft within 0.6 fracture volumes. Thereafter, the pressure gradient dropped sharply, ending at 1.8 psi/ft after injecting 3 fracture volumes of brine.

Presumably, the gel in the wormholes provided the point of failure during brine injection. This presumption was

qualitatively consistent with the pressure gradients noted near the end of brine injection. Standard calculations for laminar flow of brine in tubes or slits¹⁶ (coupled with the brine pressure gradients and flow rates) suggested that only about 10% of the gel washed out during brine injection. In contrast, if the entire gel mass had washed out, the brine pressure gradients should have been lower by a factor of 7,000. Also, at the end of the experiment (i.e., after the rate studies described below), the fracture was opened—revealing that most of the fracture was filled with concentrated gel.

The pressure gradients during brine injection at other rates are shown in Fig. 11. The open circles show the maximum pressure gradients (at a given rate), when the rates were increased in stages. Note that the maximum pressure gradient decreased for the first three rates in the sequence, and then the pressure gradients consistently rose for the higher rates. Presumably, brine displaced gel in the wormholes during brine injection at the lowest rate (Fig. 10). For the next two rate increases, significant additional erosion of the gel occurred. For subsequent rate increases, gel erosion was less significant, although some probably occurred. During brine injection at 4,130 ft/d (2,000 cm³/hr), the maximum pressure gradient was 26% less than the average pressure gradient during gel injection at the same rate (solid square in Fig. 11).

The solid circles in Fig. 11 show the maximum pressure gradients when the rates were decreased in stages. At the final rate of 413 ft/d, the maximum pressure gradient was 1.7 psi/ft—much lower than the 9.0 psi/ft value noted at the same rate for the increasing rate part of the sequence.

The open diamonds in Fig. 11 show the average pressure gradients when the rates were increased in stages. The solid diamonds show the average pressure gradients when the rates were decreased in stages. As expected, for both curves, the pressure gradients increased monotonically with increased rate. Exposure to the increasing/decreasing rate cycle caused the average pressure gradient at 413 ft/d (200 cm³/hr) to decrease by 50% (from 2.4 to 1.2 psi/ft).

Of course, the objective of this kind of gel treatment is to dramatically reduce the flow capacity of the fracture so that fluid will flow instead through the porous rock. During brine injection after gel placement, Fig. 12 plots the percent of the brine flow through the fracture versus through the matrix. At the first (and lowest) rate (206 ft/d or 100 cm³/hr), 100% of the flow occurred in the matrix, so the fracture was effectively plugged. Unfortunately, at higher rates (i.e., after the gel plug experienced some washout), most flow occurred through the fracture. The gel substantially reduced the flow capacity of the fracture throughout the various brine injection stages—by a factor greater than 500 even at the highest flow rate. However, this fact may seem of minor consolation since the fracture still dominated the flow capacity of the system.

Figs. 10-12 indicate that the greatest damage to the gel occurred during the first exposure to a pressure gradient similar to that during gel injection. Certainly, exposure to larger pressure gradients caused additional damage to the gel. However, the incremental damage was less severe than that after the first large pressure pulse (Fig. 10). This behavior is

consistent with gel of the original composition being washed out from wormholes. Presumably, larger pressure gradients were required to erode the more concentrated gel.

Guar-Borate Gel. A similar washout experiment was performed after placing the guar-borate gel in the core that was described earlier (Fig. 13). During gel injection, the pressure gradient rose to a value of 51 psi/ft (at 12 fracture volumes), followed by a gradual decline to 30 psi/ft after 100 fracture volumes of gel. During brine injection, the peak pressure gradient of 1.2 psi/ft was reached at 0.8 fracture volumes, and a dramatic decrease in pressure gradient occurred at 16 fracture volumes of brine. Thus, the guar-borate gel washed out of the fracture much easier than the 1X Cr(III)-acetate-HPAM gel. This behavior may be desirable for hydraulic fracturing since “fracture clean-up” is important in these applications. In contrast, the greater resistance to washout exhibited by the Cr(III)-acetate-HPAM gel is more desirable for water shutoff applications. Nonetheless, increased resistance to washout is needed for these gels.

Washout with Wider Fractures and More Concentrated Gels

Experiments were performed to examine how gel washout was affected by fracture width and gel concentration. Results from many of these experiments are shown in Fig. 14. The *y*-axis plots the final core permeability relative to the permeability of an unfractured core. A *y*-value of unity or less means that the fracture was basically “healed.” As the *y*-value increased above unity, the fracture became more open or conductive—indicating a greater degree of gel washout. The *x*-axis plots the steady-state pressure gradient during brine injection relative to that during gel injection. As expected, the pressure gradient during gel injection increased with decreased fracture width and with increased polymer concentration.

Three experiments were performed using our standard 1X gel (open symbols in Fig. 14). Two experiments were performed using a 2X gel (solid symbols in Fig. 14) that contained twice the HPAM and Cr(III) acetate concentrations of the 1X gel. For both the 1X and 2X gels in 0.04-in.-wide fractures, the *y*-value (core permeability ratio) began less than unity and increased moderately for pressure gradient ratios between 0.5 and 1.5. This result indicates that in a 0.04-in.-wide fracture, gel mobilization during brine injection occurred at pressure gradients similar for those during gel injection. In wider fractures (0.08- and 0.16-in.), the 1X gel experienced mobilization (steep slopes in Fig. 14) at pressure gradient ratios between 0.1 and 0.3. For the 2X gel in a 0.08-in.-wide fracture, intermediate mobilization behavior was noted.

Use of Particulates

Of course, we seek methods to maximize the pressure gradient at which gel washout occurs. Thus, we are exploring how incorporation of particulate matter into the gel affects mobilization. Preliminary studies were performed in beakers to examine properties of gels that incorporated one of six particulates, including fine mica (supplied by MI), fine nut

plug (MI), diatomaceous earth (Drilling Specialties Diaseal M), celloflakes, shredded polypropylene, and fiberglass insulation. For each particulate, suspensions were prepared in our 1X gelant, and we noted the qualitative strength and appearance of the final gel. The mica, nut plug, and diatomaceous earth were significantly denser than the gelant. High stir rates were required to suspend the particulates (1%, 3%, and 5% concentrations) in the gelant. Once the agitation rate decreased, the particulates immediately separated from the gelant. Also, although the mica and nut plug did not inhibit gelation, we were unable to form a gel with uniformly suspended particles. The diatomaceous earth changed the pH to high values (i.e., 12), so the gel never formed. The celloflakes (1% concentration) did not interfere with gelation. However, except at very high agitation rates, they were too light (low density) and did not suspend effectively in the gelant or gel. In contrast, the fiberglass insulation (0.1% to 0.2% concentrations) and the shredded polypropylene (2% concentration) formed uniform suspensions even at very low stir rates, and they did not appear to interfere with gelation. Even after agitation ceased, these particulates remained suspended quite well.

Gel extrusion and washout experiments were performed using our 1X gel that was prepared with and without 0.1%-0.2% suspended fiberglass insulation. These experiments used the same procedures described above (i.e., those associated with Fig. 14). The open symbols in Fig. 15 plot washout results for gel with no fiberglass (which are the same data shown in Fig. 14), while the solid symbols show results for gel with fiberglass. The fiberglass reduced gel washout; however, washout was still much greater than desired for the 0.16-in.-wide fracture. This behavior was also noted for gel with 1% shredded polypropylene.⁵ We will continue to explore ways to mitigate gel washout in future work.

Conclusions

1. A new model was developed to describe water leakoff from Cr(III)-acetate-HPAM gels during extrusion through fractures. This model is fundamentally different than the conventional filter cake model that was used during hydraulic fracturing. Even so, the model accurately predicted leakoff during extrusion of a guar-borate gel. The new model may be of interest in hydraulic fracturing.
2. During extrusion of a Cr(III)-acetate-HPAM gel, pressure gradients and gel dehydration were similar from 20-80°C.
3. Similar gel dehydration behavior was observed over a three-fold range of concentration for Cr(III)-acetate-HPAM gels. During extrusion, measurements of pressure gradient versus HPAM concentration paralleled those of elastic modulus versus HPAM concentration.
4. In 0.04-in.-wide fractures, gel mobilization during brine injection occurred at pressure gradients similar to those during gel injection. In wider fractures (0.08- and 0.16-in.), Cr(III)-acetate-HPAM gels experienced mobilization at lower than expected pressure gradients.
5. We explored how incorporation of particulate matter into

gel affects washout from fractures. Shredded polypropylene and fiberglass insulation dispersed well in Cr(III)-acetate-HPAM gelants and gels. In contrast, mica, nut plug, diatomaceous earth, and celloflakes experienced severe gravity segregation.

6. Incorporation of 0.1%-0.2% fiberglass insulation into Cr(III)-acetate-HPAM gels reduced gel washout during subsequent brine injection. However, improved formulations are needed to prevent washout for fractures that are wider than 0.08 in.

Nomenclature

- A_c = fraction of area contacted by concentrated gel
 A_m = fraction of area contacted by mobile gel
 C = gel or polymer concentration, g/m³
 C_o = original concentration of gel, g/m³
 G' = elastic modulus, psi, [kPa]
 $HPAM$ = concentration of HPAM, %
 h_f = fracture height, ft [m]
 K = consistency index in Eq. 14
 k = permeability, darcys [μm^2]
 k_f = fracture permeability, darcys [μm^2]
 k_{gel} = inherent permeability of gel to water, darcys [μm^2]
 L = distance across a filter cake, ft [m]
 L_f = fracture length, ft [m]
 l = length, ft [m]
 n = exponent in Equation 14
 p = pressure, psi, [kPa]
 dp/dl = pressure gradient, psi/ft [kPa/m]
 Δp = pressure difference, psi [kPa]
 R = correlation coefficient
 u_{ave} = average velocity in a fracture, ft/d [m/d]
 u_c = water leakoff rate from concentrated gel, ft/d [m/d]
 u_l = water leakoff rate, ft/d [m/d]
 u_m = water leakoff rate from mobile gel, ft/d [m/d]
 t = time, days
 t_{exp} = time since first exposure, days
 w = width, ft [m]
 w_c = fracture width with filter cake, ft [m]
 w_f = fracture width, ft [m]
 w_w = wormhole width, ft [m]
 x_o = thickness of a lubricating layer, ft [m]
 α = suspension-filter cake concentration factor
 $\dot{\gamma}$ = shear rate, s⁻¹
 $\dot{\gamma}_w$ = shear rate at the wall, s⁻¹
 μ = viscosity, cp [Pa-s]
 μ_o = viscosity of a Newtonian fluid, cp [Pa-s]
 τ_w = shear stress at the wall, psi [Pa]
 τ_{xz} = shear stress, psi [Pa]

Acknowledgments

Financial support for this work is gratefully acknowledged from the National Petroleum Technology Office of the United States Department of Energy, BP, Chevron, China National Petroleum Corp., Chinese Petroleum Corp., Intevep/PDVSA, Marathon, Phillips, Shell, and Texaco. I thank Richard

Schrader for performing the experiments and Norman Warpinski of Sandia for reviewing the new filter-cake idea in advance. I appreciated useful discussions with Jenn-Tai Liang (INEEL), Jim Morgan (BP), Robert Sydansk, Robert Lane (Northstar), and Amaury Marin (Intevep/PDVSA). Thanks also to Prentice Creel (Halliburton) for providing the components for the guar-borate gel, John Gould (Gel-Tec) for the celloflakes and shredded polypropylene, and Warren Wright (Drilling Specialties) for the diatomaceous earth.

References

1. Seright, R.S.: "Polymer Gel Dehydration During Extrusion Through Fractures," *SPEPF* (May 1999) 110-116.
2. Seright, R.S.: "Mechanism for Gel Propagation Through Fractures," paper SPE 55628 presented at the 1999 SPE Rocky Mountain Regional Meeting, Gillette, May 15-19.
3. Seright, R.S.: "Gel Propagation Through Fractures," *SPEJ* (Nov. 2001) 225-232.
4. Seright, R.S.: "Using Chemicals to Optimize Conformance Control in Fractured Reservoirs," Annual Technical Progress Report (U.S. DOE Report DOE/BC/15110-4), U.S. DOE Contract DE-AC26-98BC15110 (Sept. 2000) 3-56.
5. Seright, R.S.: "Using Chemicals to Optimize Conformance Control in Fractured Reservoirs," Annual Technical Progress Report (U.S. DOE Report DOE/BC/15110-6), U.S. DOE Contract DE-AC26-98BC15110, (Sept. 2001) 40-54.
6. Howard, G.C. and Fast, C.R.: *Hydraulic Fracturing*, Monograph Series, SPE, Dallas, (1970) 2, 32-42.
7. Howard, G.C. and Fast, C.R.: Optimum Fluid Characteristics for Fracture Extension," *Drill. and Prod. Prac.*, API (1957) 261.
8. Penny, G.S. and Conway, M.W.: "Fluid Leakoff," *Recent Advances in Hydraulic Fracturing*, Monograph Series, SPE, Richardson, (1989) 12, 147-176.
9. Mack, M.G. and Warpinski, N.R.: "Mechanics of Hydraulic Fracturing," *Reservoir Stimulation*, 3rd ed., John Wiley, New York (2000) Chapter 6.
10. Constien, V.G., et al.: "Performance of Fracturing Materials," *Reservoir Stimulation*, 3rd ed., John Wiley, New York (2000) Chapter 8.
11. Hsi, C.D. et al.: "Formation Injectivity Damage Due to Produced Water Re-injection," paper SPE 27395 presented at the 1994 SPE International Symposium on Formation Damage, Lafayette, Feb. 7-10.
12. Martins, J.P. et al.: "Long-Term Performance of Injection Wells at Prudhoe Bay: The Observed Effects of Thermal Fracturing and Produced Water Re-Injection," paper SPE 28936 presented at the 1994 SPE Annual Technical Conference and Exhibition, New Orleans, Sept. 25-28.
13. Bedrikovetsky, P. et al.: "Well Impairment During Sea/Produced Water Flooding: Treatment of Laboratory Data," paper SPE 69546 presented at the 2001 SPE Latin American and Caribbean Petroleum Engineering Conference, Buenos Aires, March 25-28.
14. Ganguly, S., et al.: "The Effect of Fluid Leakoff on Gel Placement and Gel Stability in Fractures," SPE paper 64987 presented at the 2001 SPE International Symposium on Oilfield Chemistry, Houston, Feb. 13-16.
15. Seright, R.S.: "Using Chemicals to Optimize Conformance Control in Fractured Reservoirs," Annual Technical Progress Report (U.S. DOE Report DOE/BC/15110-2), U.S. DOE Contract DE-AC26-98BC15110, (Sept. 1999) 3-52.

16. Bird, R.B., Stewart, W.E., and Lightfoot, E.N.: *Transport Phenomena*, John Wiley & Sons, New York (1960) 11, 42-63.
17. Liu, J., and Seright, R.S.: "Rheology of Gels Used for Conformance Control in Fractures," *SPEJ* (June 2001) 120-125.
18. Seright, R.S.: "Improved Methods for Water Shutoff," annual report (DOE/PC/91008-4), Prime Contract No. DE-AC22-94PC91008, Subcontract No. G4S60330, BDM-OKLAHOMA/U.S. DOE (Nov. 1997) 89-91, 223-226.

SI Metric Conversion Factors

cp x 1.0*	E-03	= Pa·s
ft x 3.048*	E-01	= m
in. x 2.54*	E+00	= cm
mD x 9.869 233	E-04	= μm ²
psi x 6.894 757	E+00	= kPa

*Conversion is exact.

Table 1—Property Comparisons for a Power-Law Fluid: New Model Prediction Divided by Conventional Model Prediction. w_c = flow opening for conventional filter cake model. w_w = wormhole width. $w_w/w_c > 1$.

	γ_w	u_{ave}	τ_w	dp/dl
Constant pressure gradient	$(w_w/w_c)^{1/(n+1)}$	$(w_w/w_c)^{(n+2)/(n+1)}$	w_w/w_c	1
Constant injection rate	w_c/w_w	1	$(w_c/w_w)^{(n+1)}$	$(w_c/w_w)^{(n+2)}$

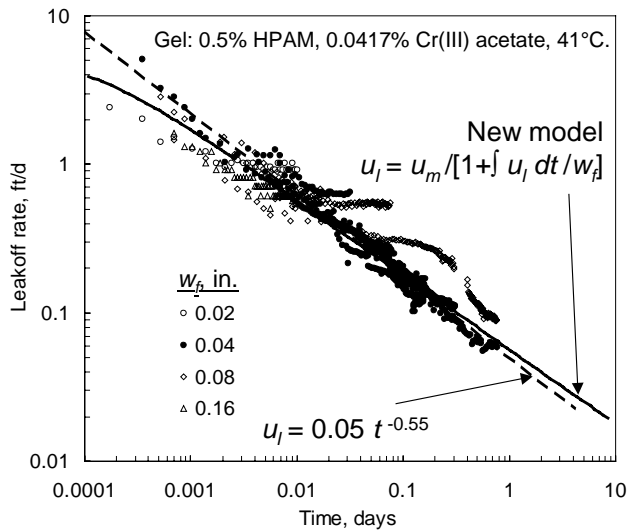


Fig. 1—Summary of leakoff data at 41°C.

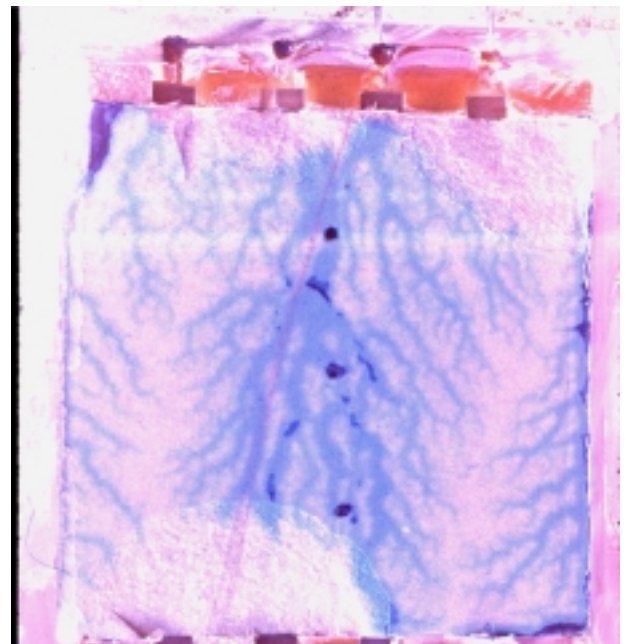


Fig. 2—Wormhole pattern during dyed gel injection following gel of the same composition (not dyed). Fracture dimensions ($L_f \times h_f \times w_f$) = 12x12x0.04-in. From Ref. 4.

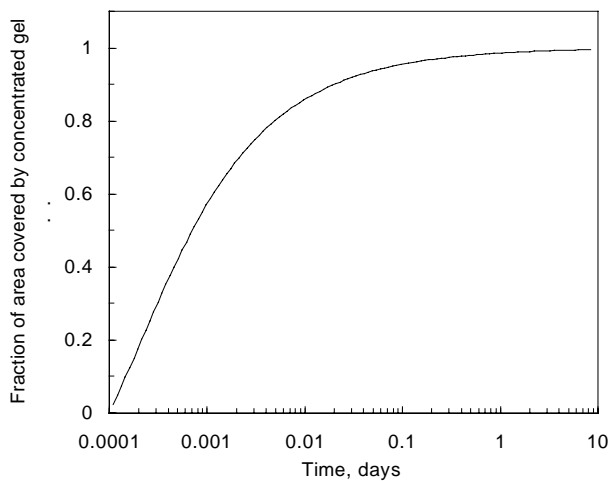


Fig. 3—Predictions of fraction of fracture area contacted by concentrated gel.

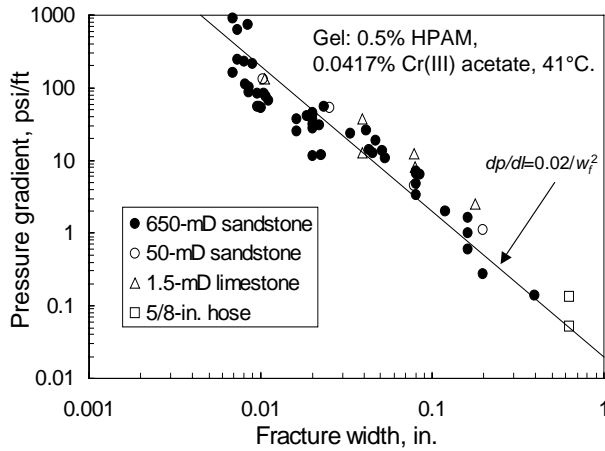


Fig. 4—Pressure gradients required to extrude gels through fractures.

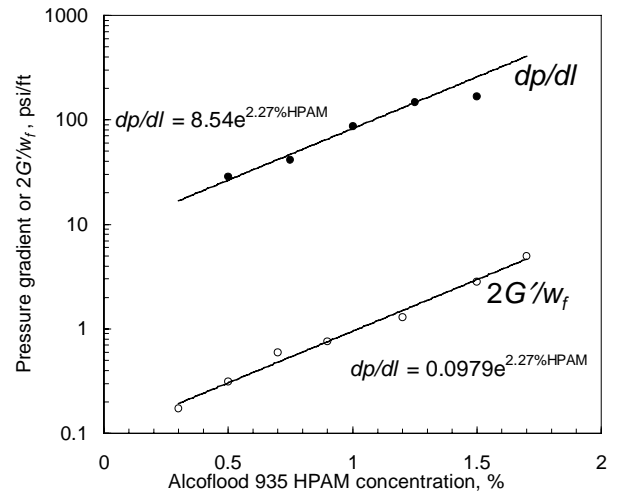


Fig. 7—Pressure gradient and elastic modulus versus HPAM concentration.

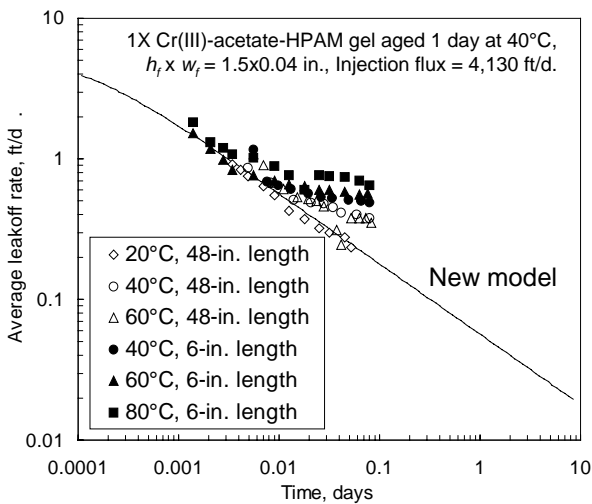


Fig. 5—Leakoff in fractures at different temperatures.

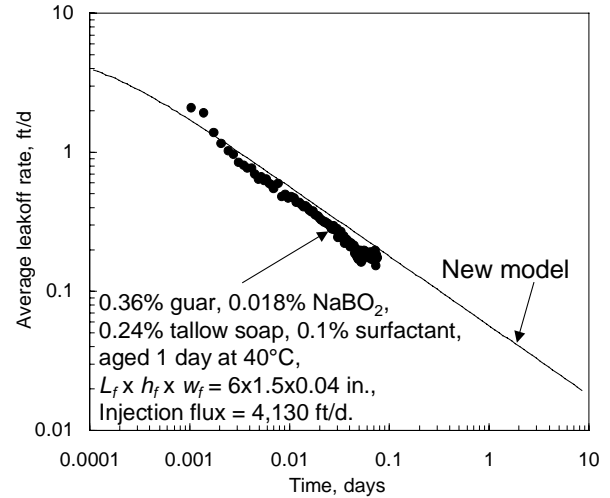


Fig. 8—Leakoff results for a guar-borate gel.

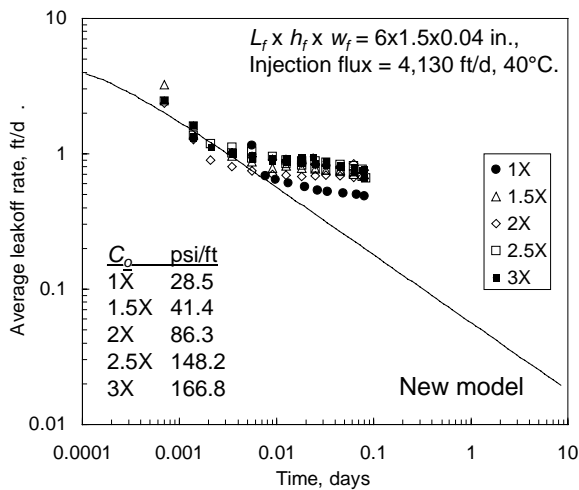


Fig. 6—Effect of gel composition during extrusion.

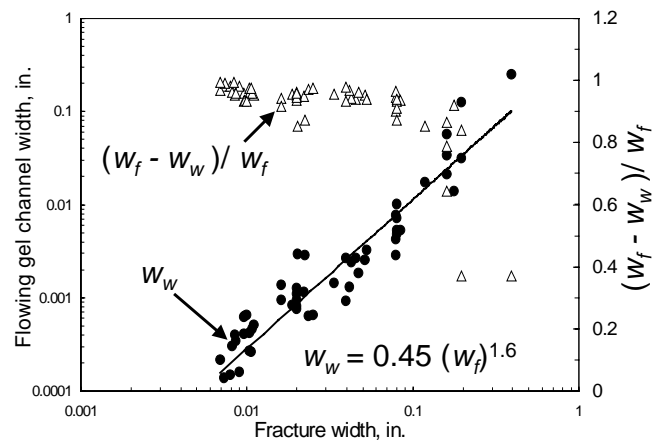


Fig. 9—Estimated flow channel width based on $w_w = 2G' / (dp/dl)$.

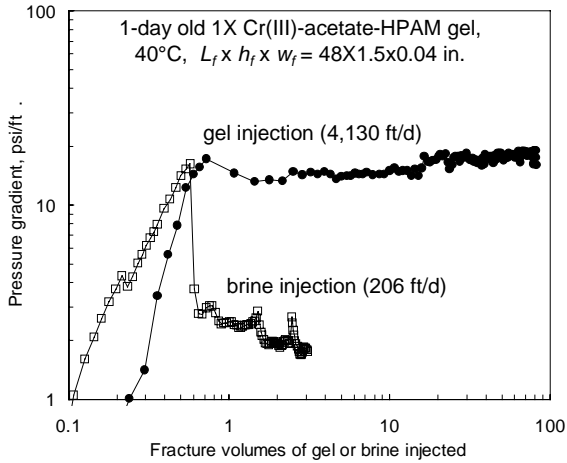


Fig. 10—Pressure gradients during gel versus brine injection.

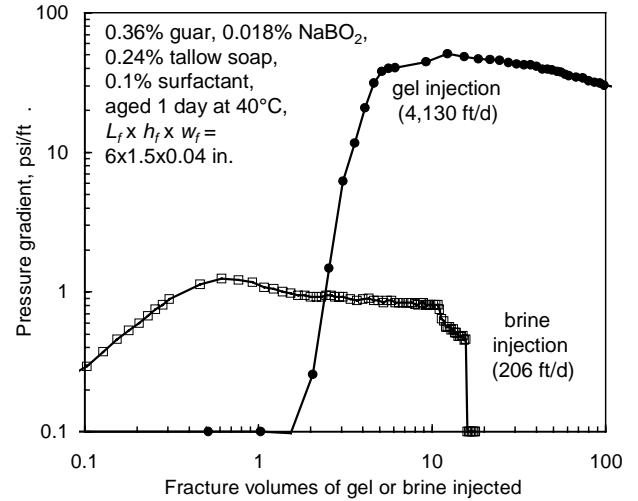


Fig. 13—Gel placement and washout for a guar-borate gel.

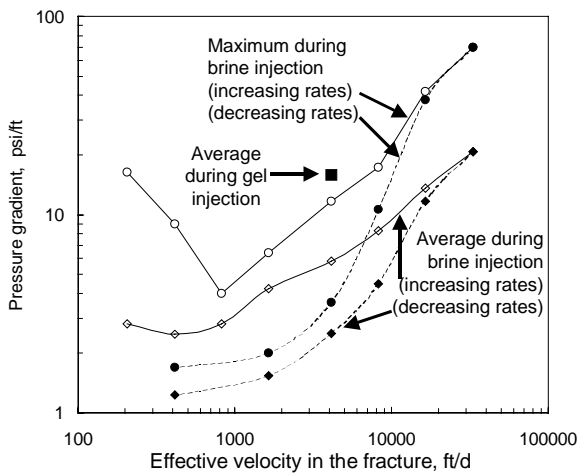


Fig. 11—Pressure gradients during brine flow at various rates.

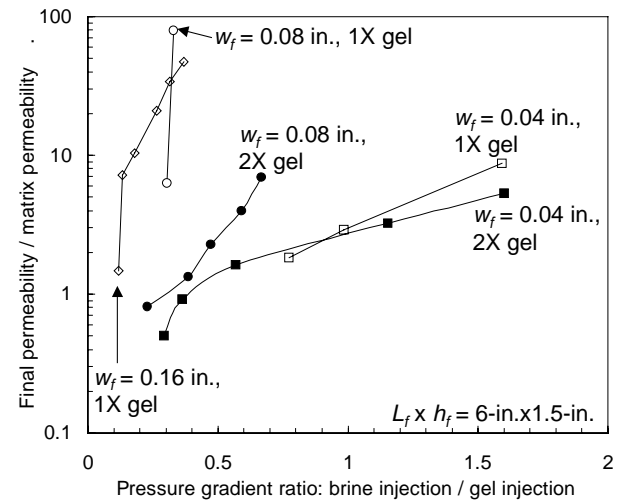


Fig. 14—Gel washout during brine injection after gel placement.

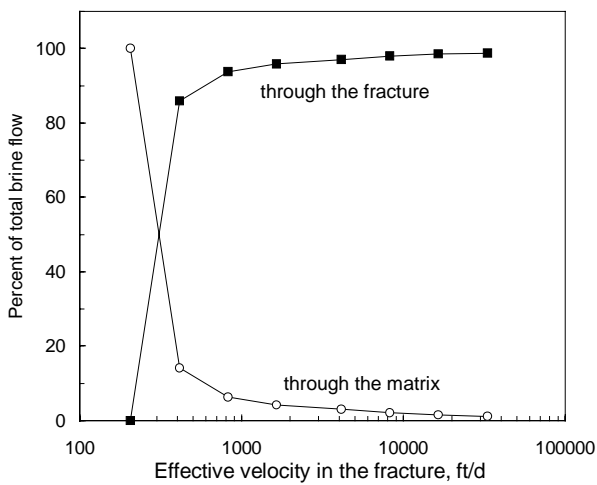


Fig. 12—Brine flow through fracture versus matrix.

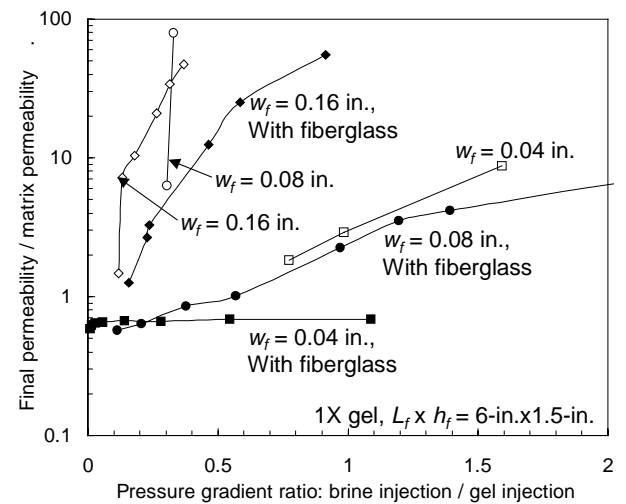


Fig. 15—Effect of 0.1%-0.2% fiberglass on gel washout.